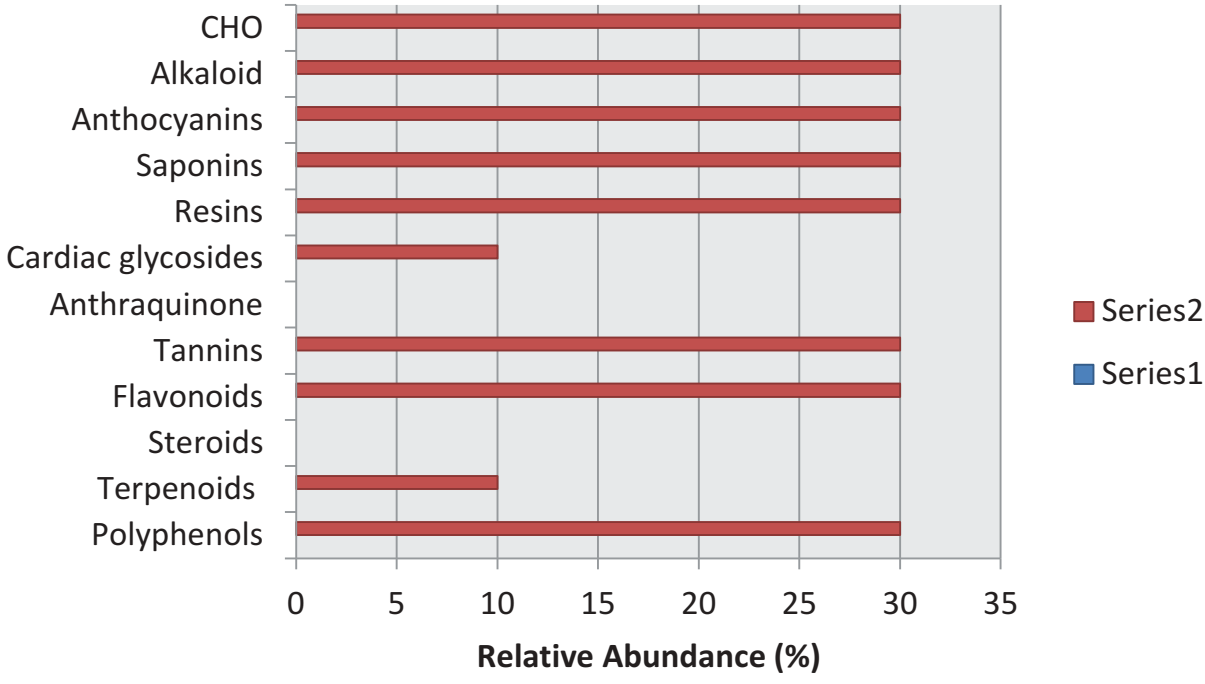

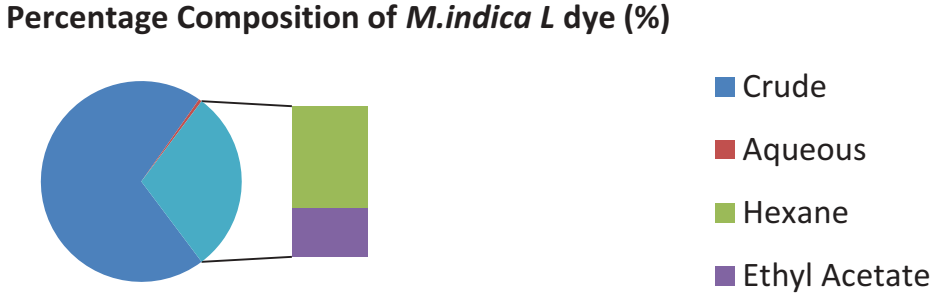

MATERIALS SCIENCE | RESEARCH ARTICLE

The interboundary properties and kinematics of N719 dye with titania photoanode framework and spectral responses with different electrolytes

Temitope J. Abodunrin, Adenike O. Boyo and Mojisola R. Usikalu

Cogent Physics (2018), 5: 1498146
cogent oa

Abodunrin et al., *Cogent Physics* (2018), 5: 1498146
https://doi.org/10.1080/23311940.2018.1498146

cogent physics

MATERIALS SCIENCE | RESEARCH ARTICLE

The interboundary properties and kinematics of N719 dye with titania photoanode framework and spectral responses with different electrolytes

Temitope J. Abodunrin[1], Adenike O. Boyo[2] and Mojisola R. Usikalu[1]

Received: 17 December 2017
Accepted: 02 July 2018
First Published: 13 July 2018

Corresponding author: Temitope J. Abodunrin, Industrial physics, Covenant University, Nigeria
E-mail: temitope.abodunrin@covenantuniversity.edu.ng

Reviewing editor:
Rajeev Ahuja, Uppsala University, Sweden

Additional information is available at the end of the article

Abstract: Titanium oxide is as ancient in age as our planet but its use for photoanode is more recent. It exists naturally as rutile (the second most abundant), anatase and brookite ores. The anatase several metastable states trigger diverse spectral responses with *Magnifera Indica Linn.* (*M.indica L*) dye as it is synthesized with an N719 dye grown on its matrix. Facile doctor blade method and high temperature sintering at 723 K were used in fabrication. Doping of titanium oxide in effect lowers the band gap of TiO_2 for photo-excitation caused by a bathochromic shift and simultaneously decreases the rate of recombination in photogenerated electron–hole pairs. This study explored the visible light induced photocatalytic action of doped *M.indica L* DSSC towards reduction of titanium oxide bandgap. The SEM micrographs reveal the molecular interactions and the interplay as electrolytes percolate the intricate N719 dye/Titania framework. Detailed analysis stem from comparison of *M.indica L* crude faction and the batch separated faction using FTIR spectroscopy. The absorbance peak, rates of reaction and % transmittance identify the particular chromophores responsible for the reaction. Result shows the batch-separated hexane faction approximately 1000 times more efficient than its crude faction although the *ff* of the crude was only about twice that of the hexane faction. The optical study showed that doping ions lead to an increase in the absorption edge wavelength, and a decrease in the band gap energy of TiO_2

ABOUT THE AUTHORS

Temitope Abodunrin is a keen researcher on materials science and specializes in dye-sensitized solar cells (DSSCs). Her objective is to solve the challenge of irregular power supply in the developing world. Thus her research interest has focused on several works on improving the optimal performance of DSSCs.

She is a member of faculty at the Covenant University, Nigeria where she lectures and researches.

She has several publications on her subject area and she continues to explore and share her views both scientifically and socially as a mentor.

She is currently rounding up her Ph.D in Renewable Energy Physics at Covenant University.

Her hobby includes reading, writing, thinking and singing.

PUBLIC INTEREST STATEMENT

Silicon solar cells dominate the market because of their high efficiency however, they are expensive. Many parts of the world are in constant darkness especially, areas far from the grid. Ironically, solar energy is as old as planet earth and produces in one hour enough joules to service humanity's annual energy needs. This energy requirement includes: electricity, domestic needs, space warming and health care. The problem of irregular energy affects all of these spheres of life. This research seeks to explore a cheaper substitute to silicon solar cells readily available in off-grid zones, non-toxic, have a facile process of manufacture and not require special disposition as expired silicon cells. Dye-sensitized solar (DSC) technology is fore amongst other technologies in these attributes but records low efficiency. This work investigates avenues for DSC efficiency boost and suggests areas for further studies.

nanoparticles. The doped TiO_2 nanoparticles in general showed higher photocatalytic activities than the pure ones.

Subjects: Chemistry; Materials Science; Physics

Keywords: energy harvesting; titanium oxide; dopants; batch-separation; efficiency

1. Introduction

Among various semiconductors, TiO_2 has been considered the most promising catalyst with many advantages including long-term stability, inexpensive, non-toxic and ability to be used in many bio-compatible forms (Wold, 1993). Its successful use is impeded by the wide energy band of titanium oxide and uncontrolled recombination with charge carriers (Naji Al Dahoudi, Qifeng, & Guozhong, 2013). Hence, recent research attention is focused on the improvement of the catalytic activities of TiO_2 catalysts through doping with diverse metal ion oxides (Horiuchi, Miura, Sumioka, & Uchida, 2004), and adaptations of the surface by introduction of metal cations. These ions are either integrated into the crystal lattice, intercalated or spread on the surface of TiO_2 as clusters or mononuclear complexes (Choi, Termin, & Hoffmann, 1994). Therefore the specific objective is to lessen the energy band gap or to create new energy levels inside the forbidden band gap. This consequently reduces the recombination processes by introducing traps for either electrons and/or holes (Shi et al., 2009).

A severe setback in the use of titanium oxide is that as a photocatalyst its band gap has a value in the near-UV range of the electromagnetic spectrum, about 3.2 eV for the anatase form (Shahid, Ul-Islam, & Mohammad, 2013). Consequently, only UV light is capable of creating electron–hole pairs and initiates the photocatalytic process. Moreover since, UV light constitutes only a miniscule portion of the e-m spectrum, the performance is restricted. Thus, a lot of research effort is directed at shifting titanium oxide's optical response to the visible light range. These past researches involved adding oxides of transition metals to boost photocatalytic action in titanium oxide. Presently, a major challenge is to process low-cost DSSCs possessing stable doped nanomaterials and with well-controlled properties that can effectively absorb visible light.

The study provides the physical and chemical properties of the synthesized photocatalysts and the doping ion influence on the photocatalytic reactions. It will also help in advancing the ongoing efforts for developing modified semiconductor photocatalysts to operate efficiently under visible light. Results have shown that titanium oxide photoelectric performance is significantly enhanced by doping with metal ions. Examples of such cations include zinc, nickel, chromium, iron and vanadium (Matsui et al., 2005). Experimental results reveal iron to be suitable due to its radius of 0.64 Å in Fe^{3+} close to the neighborhood of Ti^{4+} with a value of 0.68 Å. Hence, it is hypothetical to infer that Fe ions would easily infiltrate the crystal lattice of TiO_2 (Lai, Kong, Jenekhe, & Bard, 2003). A keen scientific outcome is in magneto-optic and spintronic technology. A lower band gap of iron (2.6 eV) effectively diminishes the band gap width of the TiO_2 and intensifies the efficiency of absorbance of the visible light (Milenkovi´C, Zvezdanovi´C, Andjelkovi´C, & Markovi´C, 2012). It is hoped that this would launch the design of systems that would be energy efficient and retain and transmit vast information, depending on the unique combination of ferromagnetic properties of the iron (Nazeeruddin et al., 1993).

The material properties seem to be strictly dependent on the crystal structure, the size of the nanoparticle and morphology, which are correlated with the TiO_2 method of synthesis (Hara et al., 2003). The most popular method the sol-gel method is employed, due to the easy technique, low price, the purity of oxides obtained and the lower synthesis temperature required (Liang et al., 2007).

In this work, we have doped the structure of *M.indica L* (as shown in Figure 1) based on TiO_2 with a mixture of HNO3/Ti molar ratio (3:5%) from standard laboratory procedure. A novelty introduced into

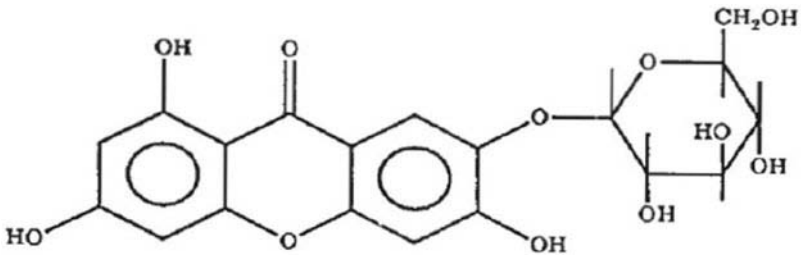

Figure 1. Indoline structure of *M.indica L* (N719) dye (Horiuchi, Miura, Sumioka and Uchida, 2004) downloaded on 26/07/17.

this doping technique was that post annealing of the samples took place at different temperatures of 300°C, 350°C and 450°C. This corroborates past research work in which the post annealing of DSSCs was done at different ambient temperatures, in order to tune the amount of oxygen vacancies in the prepared powder (Hara et al., 2004).

In order to accomplish the objective of understanding the correlation between optical and electronic properties of TiO_2: N719 dye nanoparticles. The prepared samples have been characterized by ultraviolet spectroscopy (UV/VIS), fourier transform infrared (FTIR) and scanning electron microscopy (SEM).

2. Materials and method

In this study, 1 g of *M.indica L* dye was dissolved in methanol using ratio of 1:10 of dye to methanol for phytochemical screening. This prepared dye solution was divided into sections following the procedures described by Varadharajan et al. (2016) and Zhao et al. (2008).

The sample preparation began with the harvesting of 357.5 g of *M.indica L* leaves. They were air dried in the laboratory until they assumed constant weight. The mass was determined with the PGW 453 (e) series of ADAM electronic balance. This mass was crushed to a coarse blend using a mill; it was re-weighed and then allowed to cool to prevent bacterial growth. After 3 h, the crushed leaves was soaked by immersion in 1000 ml of methanol in thin layer chromatography (TLC) tanks and covered. The choice of methanol was in order to improve the yield within the period leaf/liquor mixture was allowed to soak. This procedure lasted for 11 days to ensure adequate extraction of dye. Extraction of the dye was done with Stuart RE 300 B rotary evaporator set at a rotary speed of 55 revolutions per minute. The operating temperature was set at 45°C to preserve the chromophore. The dye extract obtained was stored in air tight Pyrex glass ware for subsequent use (Jafarzadeh, Shafiei, Ebadi, & Abdoli, 2010). The batch separation technique of *M.indica L* dye was carried out with the aid of a 1500 ml volume of Pyrex glass separating funnel. This was subsequently used to purify the feedstock. 274.8 g of crude extract (dye) was mixed in ratio 2:1(40 ml and 20 ml of hexane and ethyl acetate) respectively. This mixture was thoroughly shaken together for 10 min, allowed to settle. Distinct layers were identified from the mixture. Each layer was poured off and collected into different containers until the whole mixture was separated (Abodunrin et al., 2015).

Genesys 3600 series UV spectrophotometer was used to obtain the UV/VIS spectrographs of the dye extract, to study the maximum wavelength of absorbance within the visible spectrum of electromagnetic light under standard conditions of air mass.

The same ratio of dissolution was used for both the UV/VIS and Fourier Transform infrared (FTIR) spectroscopy. However, Shimadzu spectrophotometer was used to obtain the chromophores present in *M.indica L* dye.

The sol-gel method was used to prepare the dye extract for doctor blade application unto the photo anode. The counter electrode was made by passing concentric layers of soot over a naked Bunsen flame, in a vacuum simulated to allow uniformity of layers.

M.indica L dye sensitized solar cells were fabricated using the doctor blade method of application combined with high temperature sintering at 450°C in an autoclave. The active area of indium doped tin oxide (ITO) was 5.16 cm^2 under standard 1.5 air mass (AM) conditions.

3. Results and discussion

The outcome of this work is presented under different subsections:

3.1. Batch separation of M.indica L *dye*

Four portions were obtained from the batch separation process namely: the crude, aqueous, hexane and ethyl acetate factions. On a scale of 100%, the crude faction was 70%; aqueous had 0.5%, hexane had 20% and ethyl acetate was 9.5%.

3.2. Phytochemical screening

The quantitative phytochemical analysis divulges the constituents present in *M.indica L* as flavonoids, polyphenols, terpenoids, steroids, alkaloids, carbohydrate (CHO) and cyanins. These chromophores significantly determine the mode of charge carrier transport. A summary is presented in Table 1 (Abodunrin et al., 2015). The indoline structure which characterizes the *M. indica L* is a donor-π-acceptor ligand. This suggests hydroxyl (-OH bond) as the acceptor from atypical auxochrome methyl (CH_2OH) which is subsequently conjugated with a π-electron system. This was responsible for the observed increase in absorption of crude *M.indica L*. This accounted for a red bathochromic shift from 220 nm to 401 nm respectively as shown in Figure 2(A).

3.3. UV/VIS spectroscopy

The crude faction of *M.indica L* depicts metal-free organic behavior due to its characteristic absorption peak absorbance (λ_{max}) of 3.88 a.u at 400–550 nm wavelength in the visible region of the electromagnetic spectrum of light as illustrated in Figure 2(A). The comparison with the UV/VIS spectrograph of batch separated *M. indica L* (hexane layer) reveals a porphyrin absorption at 312 nm wavelength λ_{max} in the spectrum as shown in Figure 2(B). This UV/VIS pattern represents a hypochromic shift characterized by a shift to shorter wavelength but higher energy radiation from near UV region.

Table 1. Qualitative phytochemical analysis of *M.indica L* leaf

S/No.	Constituents	Presence
1.	Polyphenols	+++
2.	Terpenoids	+
3.	Steroids	−
4.	Flavonoids	+++
5.	Tannins	+++
6.	Anthraquinone	−
7.	Cardiac glycosides	+
8.	Resins	+++
9.	Saponins	+++
10.	Anthocyanins	+++
11.	Alkaloid	+++
12.	CHO	+++

Key: +++ (highly present); ++ (Moderately present); + (trace); −(absent)

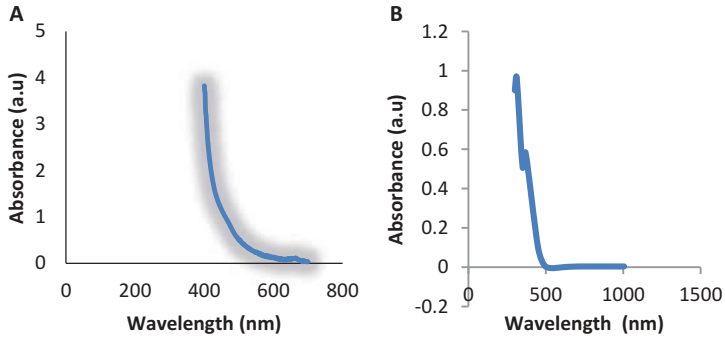

Figure 2. (A) UV/VIS spectroscopy of crude *M.indica L* dye and (B) UV/VIS of *M.indica L* hexane faction doped with K^+.

3.4. Spectral responses of M.indica L *doped with different metal ions*

The various absorption shifts describes the spectral responses obtained from *M.indica L* doped with different matal ions. The dopant ions were introduced from dissimilar electrolyte mixtures and are represented in Figure 3. The initial bathochromic (longer λ) and hypochromic shift (lower absorbance) in the wavelength and absorbance response observed in Figure 2(B) was induced by K^+ as shown. Introduction of Hg^{2+} from an aqeous solution of $HgCl_2$, resulted in a larger hypochromic shift in absorbance with a lower bathochromic shift in wavelength relative to K^+ as shown in Figure 3(A). Subsequent addition of Mn^{2+} ions from $KMmO_4$ solution sustained the bathochromic shift in wavelength but extended it from a hypochromic change in absorbance since it assumes its least value as shown in Figure 3(B). A summary of these reactions is provided in Table 2. The UV/VIS for the crude faction in Figure 2(A) to 3(B) represents an interesting bathochromic shift from near UV (220 nm; 0.8 *a.u* $\leq$ *abs.* $\leq$ 2.8 *a.u*) to the visible region of light (404 nm; abs.≈ 3.8 a.u). The absorbance becomes hyperchromic with the highest value recorded; 3.245 a.u. *M.indica L* appears violet within this region (Tsai, Chang, Kang, & Chang, 2007).

3.5. Fourier transform infrared (FTIR) spectroscopy

A comparative study of crude *M.indica L* with the hexane faction as shown in Figure 4(A) identifies 16 compounds in crude while the hexane faction shown in Figure 4(B) presents 17 compounds by the characteristic wavelength peaks. The purer faction has sharp peaks and bands while the impure faction consists of poor bands with some additional bands (Tian, Yang, & Chen, 2007). A summary of these reactions is provided in Table 3. When the infrared radiation is absorbed by *M. indica L* molecules, the only possible transitions allowed are vibrational quantum number changes of ±, which correspond to fundamental vibration tones (Hemmatzadeh & Jamali, 2015). Also this absorption occurs only as a result of the dipole moment of the whole molecule changing because of certain molecular vibrations. In addition, the *M.indica L* molecules are excited due to the infrared absorption and consequently move from lower to higher degree of vibrations. The vibrational transitions such as N–H, C=O, O–H are accompanied by a change in dipole moment and are thus

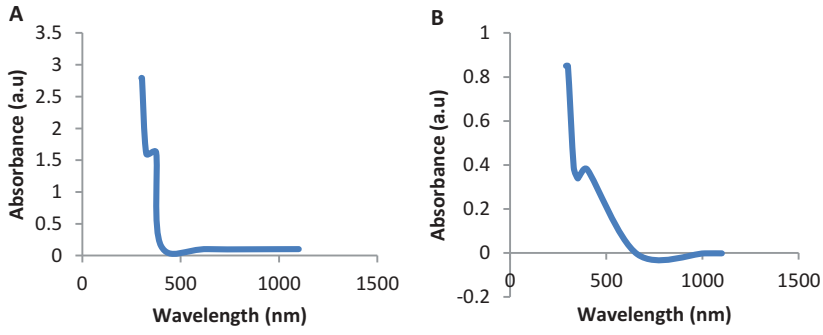

Figure 3. (A): illustrates UV/VIS of *M.indica L* hexane faction with Hg^{2+} and (B): UV/VIS of *M. indica L* (hexane faction) with Mn^{2+}.

Table 2. Illustrates the spectral responses of *M.indica L* with different sensitizers

S/No.	*M.indica L* (hexane)	λ_{max} (nm)	Absorbances (a.u)	Absorbance Shift	Descriptive Term
1.	+ K^+	312	0.964	Longer λ, lower absorbance	Bathochromic; hypochromic
2.	+ Hg^{2+}	300	2.79	Longer λ, lower absorbance	Bathochromic; hypochromic
3.	+ Mn^{2+}	300	0.85	Longer λ, lower absorbance	Bathochromic; hypochromic
4.	Crude M.indica L	404	3.245	Longer λ, greater absorbance	Bathochromic; hyperchromic

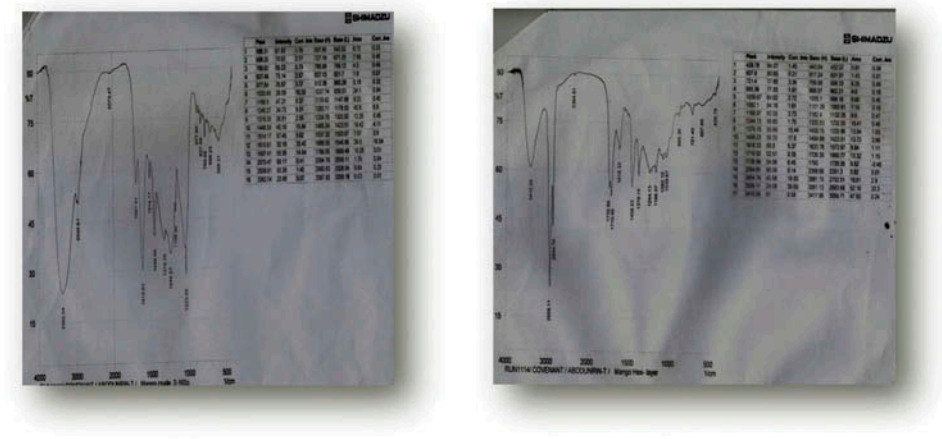

Figure 4. FTIR of *M.indica L* (a) crude faction and (b) hexane faction (Abodunrin, Obafemi, Boyo, Adebayo and Jimoh, 2015) downloaded on 30/08/17.

strongly absorbed in the IR region. Conversely, C–C bond transitions in alkene and alkyne are inactive IR transitions even though their molecule is symmetric (Wang, Yanagida, Sayama, & Sugihara, 2006).

3.6. Scanning electron microscopy (SEM) of M.indica L

The SEM micrograph reveals the microstructure of *M.indica L* leaf dye. The picture was obtained a depth of 2 nm thickness as shown in Figure 5(A)–(D), different magnifications and Width depth (WD). The outline of the chromophore of *M.indica L* doped with metal ions is recurrent in Figure 5(A)–(D).

All the micrographs were obtained at a depth of 2 nm. Figure 5(A) was magnified 25 times, several chromophores with an outline of the mango drupe is represented. There are buoyed up by liquid pressure of the electrolyte and the dye. Also several grain boundaries feature scattered all over the micrograph. Figure 5(B) represents a magnification of 30 times and some probable trap sites are illustrated. The pressure appears deflagrated at points near the edge. In Figure 5(C), the magnification is 50 times from a WD of 11.8 mm. The chromophore outlines the shape of the mango drupe. Lines of grains and boundary interface as the turgid pressure created by the electrolyte keeps them afloat. Figure 5(D) shows the same magnification but from a progression of 12.1 mm WD. The lines are more distinct as the turgid pressure can be observed at closer range. The charge transport is viewed as the trend of drift (line of fissure) portended from the centre along the edges of the micrograph.

Table 3. Functional groups present in *M.indica L* (Abodunrin, Uhuegbu, & Olugbuyiro, 2015) downloaded on 30/08/17

S/No.	*M.indica L* Crude	Compounds Present	*M.indica L* Hexane	Compound(s) Present
1.	588.31 ± 50	Weak disulphide bonds	439.78 ± 60	Weak disulphide bonds
2.	698.25	S-OR esters in strong appearance	607.6 ± 10	Strong C-H deformation in Alkynes
3.	769.62	Same as (2)	721.4 ± 25	Same as (2)
4.	827.49	Same as (2)	885.36	Strong Alkenes appearance; CH and CH_2 out of plane bending
5.	877.64	Same as (2)	1039.67	Alcohols and phenols in strong appearance; H-bonded and strong C-O broad peaks
6.	1033.88	Strong C=S thiocarbonyl bond appearance	1082.1	Same as (5)
7.	1168.9	Same as (6)	1166.97	Same as (5)
8.	1240.27	Same as (6)	1244.13	Same as (5)
9.	1319.35	Medium appearance of alkanes; CH_2 and CH_3 deformation with CH_2 rocking	1379.15	Medium appearance of Alcohols and Phenols; O-H bending in plane
10.	1448.59	Same as (9)	1458.23	Medium to strong appearance of Amines; NH_2 and NH wagging
11.	1514.17	Medium to strong amines; NH_2 scissoring and NH wagging	1618.33	Same as (10)
12.	1610.61	Same as (11)	1710.92	Strong appearance of aryl ketones
13.	1697.41 ± 5	Strong amides; C=O	1735.99	Same as (12)
14.	2075.47 ± 25	Isothiocyanates of medium appearance in N=C=S bonds	2364.81	Medium appearance of Aldehyde in C-H bonds
15.	2939.61	Strong carboxylic acids with very broad O–H peaks.	2854.74	Same as (14)
16.	3362.04	Same as (15)	2926.11	Same as (14)
17.			3410.26	Same as (14)

3.7. Photoelectric parameters of *M.indica L*

The IV curve in Figure 6 represents a stepped slope which is more identical to the theoretical hypothesis than that of Figure 7. However, the short circuit current (I_{sc}) in Figure 6 is small due to unfavorable kinematics of reaction between the doped Mn^{2+} ion and TiO_2 photoanode. This is also collaborated by the smaller open circuit voltage $V(_{oc})$. This kinematics and interboundary relationship is favorable for Figure 7 where the redox reaction translates to a higher power output for *M. indica L* DSSC with hexane faction. The IV curve in Figure 7 is an inversion of the normal; this represents a shielding effect or consequence of recombination or both factors. The stepped PV curve is as a result of partial shading which was corrected before taking subsequent readings. This

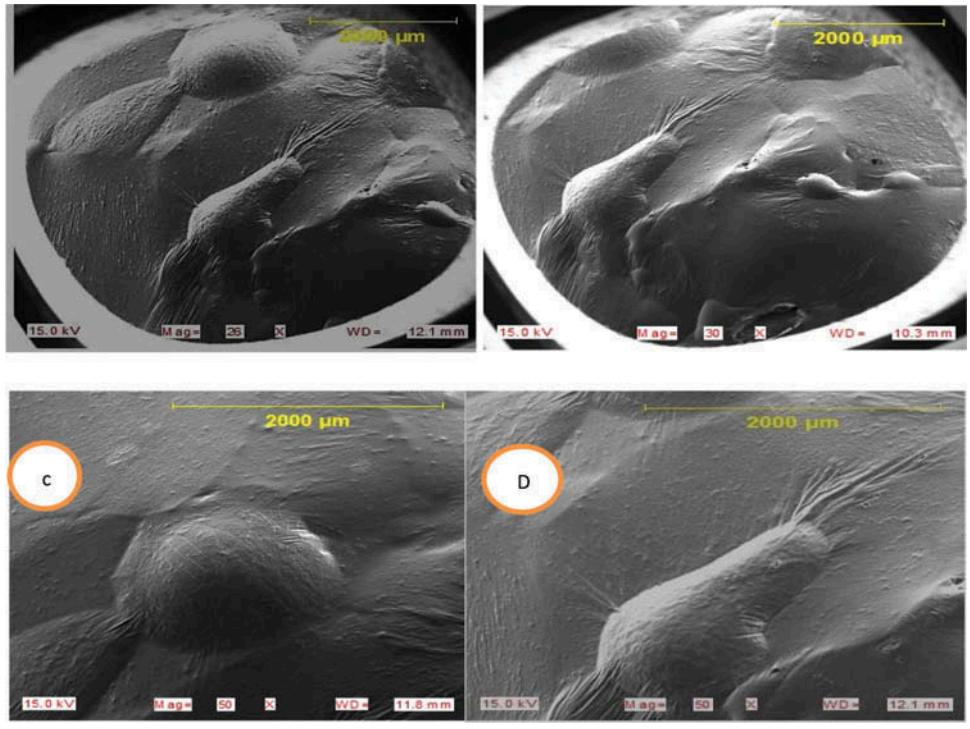

Figure 5. SEM Micrograph of *M. indica L*: in magnification of (A) 26X; (B) 30X; (C) 50X @ WD of 11.8 mm and (D) 50X mag. @ 12.1 mm.

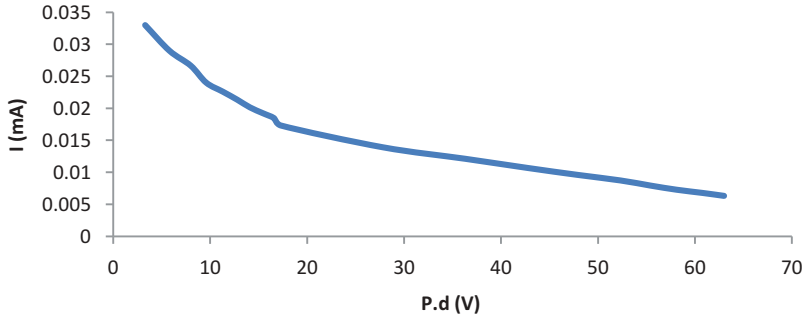

Figure 6. I-V of *M.indica L* hexane with Mn^{2+} ion.

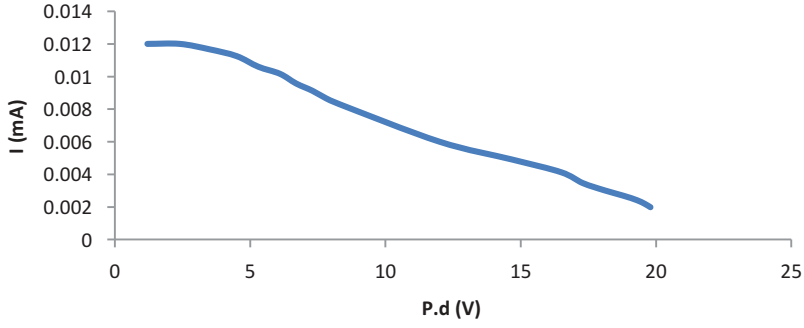

Figure 7. I-V of *M.indica L* Crude faction with Mn^{2+} ion.

explains the small value in short circuit current (I_{sc}) as shown in Table 4. The fill factor (*ff*) shows effects of dopants on the *M.indica L* matrix depicted by micro cracks in the mesoporous film. This

Table 4. Photoelectric parameters of *M.indica L* DSSCs

	***M.indica L* Crude**	***M.indica L* hexane**
I_{sc} (mA)	0.012	0.033
V_{oc} (V)	19.80	63.00
P_{max} (W)	0.056	0.213
η (%)	4.75 X 10^{-3}%	1.000
ff	0.24	0.102

could be reduced by using a sol gel of the dye. The *ff* in Figure 6 is higher than that of Figure 7. However the output efficiency is still quite low, this could be attributable to shielding of *M.indica L* crude DSSC. The crude faction has shown less interfacial kinetics which is evident even in the maximum power generated. A poor charge transfer and recombination due to obscure fissures are reasons for this reduced efficiency.

4. Conclusion

This study bears a direct relation of spectral responses to output efficiency performance in *M.indica L* DSSCs. The improved output in hexane-DSSCs could be attributed to the process of batch separation which refined the DSSCs such that the charge transport was more efficient in the hexane faction. This is as a result of removal of unwanted factions which could produce trap sites and recombination losses. Thus the hexane faction doped with Mn^{2+} ion generated more spectral responses which is attributable to better interboundary bonding and kinematics within the titania framework and Mn^{2+} ion relative to other ions. The efficiency of 1% yield in the hexane DSSCs is promising and suitable for subsequent research for micro-energy generation. A comparison to the crude DSSCs proves the presence of impurities not dopants reduced the efficiency considerably.

Acknowledgements
The authors wish to acknowledge the contribution of the technologists in physics and chemistry laboratories at Covenant University, Ota.

Funding
This work was supported by the Covenant University [CUCRID 2016].

Author details
Temitope J. Abodunrin[1]
E-mail: temitope.abodunrin@covenantuniversity.edu.ng
ORCID ID: http://orcid.org/0000-0001-9109-277X
Adenike O. Boyo[2]
E-mail: nikeboy@yahoo.com
Mojisola R. Usikalu[1]
E-mail: mojisola.usikalu@covenantuniversity.edu.ng
[1] Physics Department, Covenant University, Nigeria.
[2] Physics Department, Lagos State University, Ojo, Nigeria.

Cover Image
Source: Phytochemical Analysis Result of *M.indica L* extract.

Citation information
Cite this article as: The interboundary properties and kinematics of N719 dye with titania photoanode framework and spectral responses with different electrolytes, Temitope J. Abodunrin, Adenike O. Boyo & Mojisola R. Usikalu, *Cogent Physics* (2018), 5: 1498146.

References

Abodunrin, T. J., Obafemi, O., Boyo, A. O., Adebayo, T., & Jimoh, R. (2015). The effect of electrolyte on dye sensitized solar cells using natural dye from mango (*M.* indica L.) Leaf as Sensitizer. *AMPC*, *5*, 205–213.

Abodunrin, T. J., Uhuegbu, C. C., & Olugbuyiro, J. A. O. (2015). Phytochemical analysis of leaf-extracts from eight tropical trees: Prospects for environmentally-friendly dye compounds for smart windows. *IJSER*, *6*(3), 682.

Choi, W. Y., Termin., A., & Hoffmann, M. R. (1994). The role of metal ion dopants in quantum-sized TiO2: Correlation between photo-reactivity and charge carrier recombination dynamics. *The Journal of Physical Chemistry*, 98, 13669–13679. doi:10.1021/j100102a038

Hara, K., Dan-Oh, Y., Kasada, C., Ohga, Y., Shinpo, A., Suga, S., … Arakawa, H. (2004). Effect of additives on the photovoltaic performance of coumarin-dye-sensitized nanocrystalline TiO2 solar cells. *Langmuir*, *20*, 4205–4210.

Hara, K., Kurashige, M., Dan-Oh, Y., Kasada, C., Shinpo, A., Suga, S., … Arakawa, H. (2003). Design of new coumarin dyes having thiophene moieties for highly efficient organic-dye sensitized solar cells. *New Journal of Chemistry*, *27*, 783–785.

Hemmatzadeh, R., & Jamali, A. (2015). Enhancing the optical absorption of anthocyanins for dye-sensitized solar cells. *JRSE*, *7*(1), Article I013120.

Horiuchi, T., Miura, H., Sumioka, K., & Uchida, S. (2004). High efficiency of dye-sensitized solar cells based on metal-free indoline dyes. *Journal of the American Chemical Society*, *126*(39), 12218–12219.

Jafarzadeh, S., Shafiei, A., Ebadi, M., & Abdoli, M. (2010). Batch separation of Styrene/Ethyl Benzene/Water dispersions. *IJCHE*, *7*(4), 22-28.

Lai, R. Y., Kong, X., Jenekhe, S. A., & Bard, A. J. (2003). Synthesis, cyclic voltammetric studies, and electrogenerated chemiluminescence of a new phenylquinoline-biphenothiazine donor–acceptor molecule. *Journal of the American Chemical Society*, *125*, 12631–12639.

Liang, M., Xu, W., Cai, F., Chen, P., Peng, B., Chen, J., & New, L. Z. (2007). Triphenylamine-based organic dyes for efficient dye-sensitized solar cells. *The Journal of Physical Chemistry C*, *111*, 4465–4472.

Matsui, M., Hashimoto, Y., Funabiki, K., Jin, J., Yoshida, T., & Minoura, H. (2005). Application of nearinfrared absorbing heptamethine cyanine dyes as sensitizers for zinc oxide solar cell. *Synthetic Metals*, *148*, 147–153.

Milenkovi´C, S. M., Zvezdanovi´C, J. B., Andjelkovi´C, T. D., & Markovi´C, D. Z. (2012). The identification of chlorophyll and its derivatives in the pigment mixtures: HPLC-chromatography, visible and mass spectroscopy studies. *Advance Technologies*, *1*(1), 16–24.

Naji Al Dahoudi, N., Qifeng, Z., & Guozhong, C. (2013). Low-temperature processing of titanium oxide nanoparticles photoanodes for Dye-sensitized solar cells. *Journal of Renewable Energy*, *2013*, 1–8.

Nazeeruddin, M. K., Kay, A., Rodicio, I., Humpbry-Baker, R., Miiller, E., Liska, P., … Grätzel, M. (1993). Conversion of light to electricity by cis-X2bis(2,2′-bipyridyl-4,4′-dicarboxylate)ruthenium(II) charge-transfer sensitizers (X = Cl−, Br-, I−, CN−, and SCN −) on nanocrystalline titanium dioxide electrodes. *Journal of the American Chemical Society*, *115*, 6382–6390.

Shahid, M., Ul-Islam, S., & Mohammad, F. (2013). Recent advancements in natural dye applications: A review. *Journal of Cleaner Production*, *53*, 310–331.

Shi, J., Peng, S., Pei, J., Liang, Y., Cheng, F., & Chen, J. (2009). Quasi-solid-state dye-sensitized solar cells with polymer gel electrolyte and triphenylamine-based organic dyes. *ACS Applied Materials & Interfaces*, *1*(4), 944–950.

Tian, H. N., Yang, X. C., & Chen, R. K. (2007). Phenothiazine derivatives for efficient organic dye-sensitized solar cells. *Chemical Communications*, *36*, 3741–3743.

Tsai, Y.-L., Chang, -C.-C., Kang, -C.-C., & Chang, T.-C. (2007). Effect of different electronic properties on 9-aryl-substituted BMVC derivatives for new fluorescence probes. *Journal of Luminescence*, *127*, 41–47.

Varadharajan, V., Janarthanan, U. K., & Krishnamurthy, V. (2016). Physicochemical, phytochemical screening and Profiling of secondary metabolites of *Annona Squamosa* leaf extract. *Journal of Pharmacognosy and Phytochemistry*, *5*(2), 200–203.

Wang, Z. S., Yanagida, M., Sayama, K., & Sugihara, H. (2006). Electronic-insulating coating of $CaCO_3$ on TiO_2 electrode in dye-sensitized solar cells: Improvement of electron lifetime and efficiency. *Chemistry of Materials*, *18*(12), 2912–2916.

Wold. (1993). Photocatalytic properties of TiO2. *Chemistry of Materials*, *5*, 280–283.

Zhao, D., Peng, T., Lu, L., Cai, P., Jiang, P., & Bian, Z. (2008). Effect of annealing temperature on the photoelectrochemical properties of dye-sensitized solar cells made with mesoporous TiO_2 nanoparticles. *The Journal of Physical Chemistry C*, *112*(22), 8486–8494.